Silver(I) complexes with nitrile ligands: new materials with versatile applications.

Karolina Gutmańska[a], Piotr Szweda[b], Marek Daszkiewicz[c], Tomasz Mazur[d], Konrad Szaciłowski[d], Anna Ciborska[a], Anna Dołęga[a*]

[a] *Department of Inorganic Chemistry, Chemical Faculty,*
*Gdansk University of Technology, Narutowicza 11/12, 80-233 Gdansk, Poland *anndoleg@pg.edu.pl*
[b] *Department of Pharmaceutical Technology and Biochemistry, Gdańsk University of Technology, Narutowicza 11/12, 80-233 Gdańsk, Poland*
[c] *Institute of Low Temperature and Structure Research, Polish Academy of Sciences, Okólna St. 2, 50-422 Wrocław, Poland*
[d] *Academic Centre for Materials and Nanotechnology, AGH University of Science and Technology,*
Department of Semiconductors Photophysics and Electrochemistry
Kawiory St. 30, 30-059 Krakow, Poland

ABSTRACT

In the present study, the structure, thermal stability, conductive properties and antimicrobial activity of silver(I) complexes with nitrile ligands were investigated. For the construction of the materials 2-cyanopyridine (2-cpy), 4-cyanopyridine (4-cpy) 1,2-dicyanobenzene (1,2-dcb) and 1,3-dicyanobenzene (1,3-dcb) were used in addition to the silver nitrite and nitrate. Four new compounds were isolated and structurally characterized: one molecular complex $[Ag_4(1,2\text{-}dcb)_4(NO_3)_4]$, two 1-D coordination polymers $[Ag_2(2\text{-}cpy)_2(NO_2)_2]_\infty$, $[Ag_3(1,3\text{-}dcb)_2(NO_3)_2]_\infty$ and one 3-D coordination polymer $[Ag(4\text{-}cpy)(NO_2)]_\infty$. The results indicate that the low thermal stability of nitrite complexes is accompanied by very good antimicrobial properties against the tested bacterial and fungal strains. The presence of weakly coordinating CN groups increases the efficiency of the release of silver ions into the bacterial and yeast cell environments. Moreover, these materials exhibit unusual electrical properties in thin layer devices.

Keywords: Silver(I) complexes; Nitriles; X-ray crystal structures; Antimicrobial activity; Conductivity

1. Introduction

Elemental silver and its salts have been known for centuries as effective antibacterial agents.[1] Simple aqueous solution of $AgNO_3$, is still routinely used for the prophylaxis of ophthalmia neonatorum in infants[2,3] being effective in a concentration of 0.1%.[2] Silver sulfadiazine, an effective treatment of heavy burns, is considered an essential medicine by the World Health Organization.[4] Antimicrobial silver dressings prevent or treat infections in a wide range of acute and chronic wounds.[5] Moreover, while active against a wide spectrum of microorganisms, silver ions are relatively non-toxic towards human cells.[1]

The construction of silver complexes with the best bactericidal, fungicidal or anticancer properties comes down to basic parameters considered at the initial stage of the synthetic effort. These include solubility, stability in water, lipophilicity, redox reactivity, and the release rate of silver ions. These

properties can be controlled by the selection of suitable ligands or by using biodegradable and biocompatible particle transport media. There are several groups of organic molecules that have been tested to form such compounds. As silver(I) is electron-deficient, it readily combines with electron-donating groups, commonly N-, O- and P-donors. The important group of ligands includes N-heterocyclic compounds, N-heterocyclic carbenes, phosphines and amino acids.[6] On the other hand compounds containing thiol groups −SH neutralize the activity of silver nitrate against *Pseudomonas aeruginosa*.[7]

Silver compounds with N-heterocyclic ligands are widely recognized as antimicrobial agents.[3,7-9] Substantial number of antimicrobial silver compounds are phosphine complexes and mixed-ligand compounds including for example tetrazole or sulfonates in addition to phosphine groups.[4,11]

The use of carbenes and their stabilisation by introducing N-donor ligands resulted in molecular inert carbene complexes of silver,[12] which may be transported into the cells and release Ag^+ into the intracellular environment. Driven by this mechanism of action, carbene-silver complexes were modified so as to optimize the activity/cytotoxicity of the compounds.[13] Modifications included the addition of side chains and counterions *e.g.* CH_3COO^-, Cl^-.[13.14] In recent years, silver(I) (as well as other metals) carbene complexes have been extensively studied for their antitumor effects comparable to that of the complexes with gold, platinum or copper.[15]

The increased antimicrobial activity of nitrile complexes of silver resulting from the facile release of Ag^+ ions from the labile complexes was originally proposed by Han and co-workers.[16] So far, we have obtained and described the molecular structures of a number of molecular compounds and coordination polymers linked by cyanopyridine and dicyanobenzene ligands and initially, we investigated their luminescent properties.[17] Within the present study, we are expanding the library of the nitrile complexes of silver with new molecular and polymeric species. Moreover, we study the antimicrobial activity of the large group of silver nitrile complexes and juxtapose the results with the antimicrobial activity of simple silver salts and organic nitriles.

On the other hand, this starting point *i.e.* the synthesis of the materials with relatively labile metal ions inspired us to investigate yet another possible property and application of these compounds. In addition to their "traditional" application as antimicrobial agents, we describe the results of preliminary research on the possibility of the formation of conductive filaments upon electrical stimulation of thin layers of nitrile silver complexes. The reversible change of the conductive properties may lead to the applications very different from our initial idea such as thin-layer memristors.[18] Nevertheless, anti-bacterial and anti-fungal properties are undoubtedly an added value to every possible material application.

2. Materials and methods

2.1 General information about the chemicals

The following chemicals were used as purchased: silver(I) nitrate(V) AgNO$_3$, p.a., POCh; sodium nitrate(III) NaNO$_2$, p.a., B&K; 2-cyanopyridine (2-cpy); 4-cyanopyridine (4-cpy); 1,2-dicyanobenzene (1,2-dcb); 1,3-dicyanobenzene (1,3-dcb), acetonitrile, 99.9%, Merck; toluene, p., POCh; ethanol, 99.8%, POCh. AgNO$_2$ crystals were obtained as described previously[19] and stored in a dark place.

2.2 Synthetic procedures

The cyanopyridine complexes crystallize after few days up to two weeks from the initial solutions (recipes below). The dicyanobenzene complexes crystallize after one to two months. The removal (evaporation) of acetonitrile (compounds **1**, **2**) or EtOH (**4**) from the initial solution accelerates crystallization of the complexes.

[Ag(4-cpy)(NO$_2$)]$_\infty$ (1) Complex **1** was synthesized by the addition of 4-cyanopyridine (0.12 g, 1.2 mmol) in acetonitrile (4 mL) to AgNO$_2$ (0.09 g, 5.8 mmol) solution in hot water (8 mL). The reaction mixture was stirred and left for crystallization. A white crystalline product was obtained in the form of blocks, yield 54%; m.p. 144.9°C. Elemental analysis of C$_6$H$_4$AgN$_3$O$_2$: calcd. N 16.29, C 27.93, H 1.56; found N 16.12, C 27.86, H 1.56. FT-IR: 3109(w), 3091(w), 3064(w), 3044(w), 2250(m), 1599(s), 1553(w), 1494(w), 1417(m), 1330(m), 1288(m), 1240(vs), 1225(vs), 1213(vs), 1194(s), 1069(m), 1005(m), 962(w), 819(s), 759(w), 785(m), 558(s) cm^{-1}.

[Ag$_2$(2-cpy)$_2$(NO$_2$)$_2$]$_\infty$ (2) Complex **2** was synthesized in the same way as complex **1**, with the use of 2-cpy instead of 4-cpy, white crystalline product was obtained in the form of blocks/needles, yield 71%; m.p. 106-107°C . Elemental analysis of C$_{12}$H$_8$AgN$_5$O$_2$: calcd. N 19.14, C 38.94, H 2.25; found N 19.14, C 38.94, H 2.26. FT-IR: 3440 (w), 3091(m), 3071(w), 3018(w), 2236(m), 1586(vs), 1570(w), 1466(s), 1431(s), 1272(vs), 1252(vs), 1207(m), 1153(w), 1093(m), 1051(m), 1003(s), 913(w), 828(w), 780(vs), 738(w), 637(w), 548(s) cm^{-1}.

[Ag$_3$(1,3-dcb)$_2$(NO$_3$)$_2$]$_\infty$ (3) Complex **3** was synthesized in the form of a mixture of products by the addition of solution 1,3-dicyanobenzene (0.068 g, 0.53 mmol) in toluene (7 mL) to AgNO$_3$ (0.09 g, 0.53 mmol) solution in ethanol (7 mL). The reaction mixture was stirred and left for crystallization. Crystals of **3** were separated under the optical microscope. Due to the difficulties with the separation of pure complex, the product **3** was characterized exclusively by X-ray diffraction and FT-IR spectroscopy and the yield of the reaction was not determined. FT-IR: 3108(w), 3077(m), 3045(w), 2926(w), 2264(w), 2238(m), 1601(w), 1575(w), 1483(s), 1459(s), 1426(s), 1297(vs), 1179(w), 1021(w), 921(w), 905(w), 807(m), 673(m) cm^{-1}.

[Ag$_4$(1,2-dcb)$_4$(NO$_3$)$_4$] (4) Complex **4** was synthesized in the same way as complex **3** with the use of 1,2-dcb instead of 1,3-dcb. Colourless crystalline product was obtained in the form of blocks, yield 40%; m.p. 128.5-129°C. Elemental analysis of C$_{16}$H$_8$Ag$_2$N$_6$O$_6$: calcd. N 14.10, C 32.24, H 1.35; found N

13.98, C 32.28, H 1.41. FT-IR (crystalline product): 3094(w), 3074(w), 3028(w), 2963(w), 2258(m), 2245(m), 1585(w), 1482(w), 1422(m), 1379(m), 1293(vs), 1261(s), 1228(w), 1211(m), 1168(m), 1089(w), 1034(m), 967(m), 817(m), 792(s), 776(s), 709(w) cm^{-1}.

For the synthesis of compounds: **[Ag(3-cpy)$_2$(NO$_2$)]**, **[Ag$_3$(3-cpy)$_2$(NO$_2$)$_3$]$_\infty$**, **[Ag(3-cpy)$_2$NO$_3$]$_\infty$**, **[Ag$_2$(1,4-dcb)(NO$_3$)$_2$]$_\infty$**, whose thermal, antimicrobial and electrical (**[Ag$_3$(3-cpy)$_2$(NO$_2$)$_3$]$_\infty$**) properties were studied within this work, please refer to Gutmańska and co-workers.[17]

2.3 Physico-chemical methods

FT-IR spectra were recorded for the pure, crystalline products using Nicolet iS50 equipped with Specac Quest diamond ATR device. All FT-IR spectra were collected and formatted by OMNIC software. Elemental CHNS analyses were performed on a Vario EI Cube Elemental Analyzer. Melting point of the compounds were determined by Stuart Scientific SMP3.

2.4 Crystallography

The crystal structure data of **1**, **3** and **4** were collected on an IPDS 2T dual beam diffractometer (STOE & Cie GmbH, Darmstadt, Germany) at 120.0(2) K with MoK$_\alpha$ radiation of a microfocus X-ray source (GeniX 3D Mo High Flux, Xenocs, Sassenage, France). Crystals were cooled using a Cryostream 800 open flow nitrogen cryostat (Oxford Cryosystems).

Data collection and image processing for **1**, **3**, **4** were performed with X-Area 1.75.[20] Intensity data were scaled with LANA (part of X-Area) in order to minimize differences of intensities of symmetry-equivalent reflections (integration method). The structures were solved using intrinsic phasing procedure implemented in SHELXT and all non-hydrogen atoms were refined with anisotropic displacement parameters by full-matrix least squares procedure based on F^2 using the SHELX–2014 program package.[21] The Olex[22] and Wingx[23] program suites were used to prepare the final version of CIF files.

The X-ray diffraction data of **2** were collected at room temperature on Oxford Diffraction four circle single crystal diffractometer equipped with a CCD detector using graphite-monochromatized MoKα radiation (λ = 0.71073 Å). The raw data were treated with the CrysAlis Data Reduction Program (version 1.171.39.46). The intensities of the reflections were corrected for Lorentz and polarization effects. Absorption correction was applied by taking into account the unit cell content and optimizing the crystal shape.

Hydrogen atoms in **1-4** were refined using isotropic model with U$_{iso}$(H) 1.2 U$_{eq}$(C). Olex [22] and Mercury[24] were used to prepare all figures.

Table 1 Crystallographic data for compounds **1**–**4**.

Complex	1	2	3	4
Formula	$C_6H_4AgN_3O_2$	$C_{12}H_8AgN_5O_2$	$C_{16}H_8Ag_2N_6O_6$	$C_{16}H_8Ag_2N_6O_6$
Formula weight	257.99	362.10	596.02	596.02
Temperature (K)	120	295	120	120
Wavelength (Å)	0.71073	0.71073	0.71073	0.71073
Crystal system	Orthorhombic	Orthorhombic,	Monoclinic	Monoclinic
Space group	$P2_12_12_1$	$Pna21$	$I\,a$	$P2_1/n$
a (Å)	6.5686(7)	12.9728(2)	14.721 (4)	6.9787 (14)
b (Å)	9.2584(6)	11.8412(2)	3.7081 (11)	24.173 (3)
c (Å)	12.6650(8)	9.14655(16)	33.908 (7)	11.1205 (18)
α (°)	90	90	90	90
β (°)	90	90	93.130 (18)	91.562 (15)
γ (°)	90	90	90	90
V (Å)	770.22(11)	1405.04(4)	1848.2 (8)	1875.3 (5)
Z	4	2	4	4
Crystal size (mm)	0.23× 0.20 × 0.13	0.237 × 0.133 × 0.125	0.32 × 0.22 × 0.07	0.14 × 0.11 × 0.09
T_{min}, T_{max}	0.594, 0.740	0.723, 0.846	0.575, 0.841	0.773, 0.845
μ (mm^{-1})	2.57	1.442	2.17	2.14
Absorption correction	Integration	Gaussian	Integration	Integration
Reflections collected/unique/unique[I > 2r(σ)]	7408, 1500, 1484	37767, 3210, 2581	11298, 3731, 2242	16658, 3685, 3308
R_{int}	0.021	0.027	0.072	0.019
Data/restraints/parameters	1500/0/111	3210/1/181	3731/2/272	3685/0/271
Goodness of fit (GOOF) on F^2	1.027	1.070	0.994	1.016
Final R indices [I > 2r(σ)]	R1 = 0.0235 wR2 = 0.0615	R1 = 0.0422 wR2 = 0.0656	R1 = 0.0538 wR2 = 0.1273	R1 = 0.0179 wR2 = 0.0426
R indices (all data)	R1 = 0.0237 wR2 = 0.0616	R1 = 0.0299 wR2 = 0.0721	R1 = 0.962 wR2 = 0.1538	R1 = 0.0219 wR2 = 0.0439
Δρmax, Δρmin (e Å^{-3})	0.52 / − 0.50	0.526 / − 0.589	1.09 / − 0.97	0.32 / − 0.38
CCDC numbers	2254449	2254450	2254451	2254452

2.5 Thermal stabilities

TGA-DTA thermal analysis was performed using an SDT 650 thermoanalyser from TA Instruments. Thermograms were recorded in a synthetic air atmosphere with a heating rate of 10 °C/min to 1000°C. The mass of samples used in the analyses was within 8–40 mg. Obtained thermoanalytical curves were analysed using Origin computational program (version 9.0, OriginPro).

2.6 Antimicrobial test

Silver(I) complexes and ligands were tested for their antimicrobial activity against five reference strains of bacteria, including two strains of Gram-positive staphylococci, namely *S. aureus* ATCC 25923 and *S. aureus* ATCC 29213 and three strains of pathogenic Gram-negative bacteria, namely *P. aeruginosa* ATCC 27853, *E. coli* ATCC 25922, *S. enterica* PCM 2266. Moreover, the antimicrobial potential of synthesized agents was evaluated against two reference strains of yeasts pathogens *C. albicans* SC5314 and *C. glabrata* DSM II 226.

Two different assays: determination of minimum inhibitory concentration (MIC) of the substances of interest towards the bacterial strains growing in suspension and determination of growth inhibition zones on agar media (agar disc-diffusion method) were applied for assessment of antibacterial and antifungal activity of synthesized compounds.

The MICs values were determined in 96-wells titration plates by the two-fold broth microdilution method according to the CLSI standard methodologies.[25,26] For all compounds the activity was evaluated in the range of concentrations from 256.0 to 0.5 µg/mL The assay was performed using Mueller Hinton Broth (MHB) (Sigma-Aldrich) for bacteria and RPMI 1640 medium supplemented with 2% glucose and buffered to pH 7.0 with a MOPS buffer (3-*N*-morpholinopropanesulfonic acid) for yeasts. The plates were incubated 24 h under static conditions at 37°C. The growth intensity (optical density of the medium in the wells) of bacteria/yeasts was measured using a Victor3 Plate reader (Perkin Elmer, Waltham, MA, USA). The lowest concentration of the compound that caused at least 90% growth inhibition of bacteria/yeast (compared to the growth observed in MHB/RPMI medium not supplemented with any compound) was taken as a MIC value.

In the other assays the Petri plates (φ=90mm) with Mueller Hinton Agar 2 (for bacteria) or RPMI medium solidified with 2% agar (for yeasts) were inoculated by reference strains of bacteria/yeasts. The inoculation was performed by streaking with a sterile cotton swab soaked in a suspension of each tested reference strain of microorganisms (final optical density of each suspension OD_{600} = 0.1) freshly prepared in sterile PBS (phosphate buffered saline, pH 7.4). Subsequently up to six paper discs (φ=5mm) soaked in 20 µl of solution of the silver(I) complexes (10.24 mg/mL) were placed on the surface of the inoculated agar medium. Plates were incubated over night at 37 °C and zones of growth inhibition of bacteria/yeasts around the discs were observed and measured.

The Minimum Inhibitory Concentration (MIC) was determined using liquid medium—Mueller-Hinton Broth 2 (MHB2, Sigma Aldrich) The resulting complexes were studied by determining minimum inhibitory concentrations (MICs) and zones of inhibition on agar media. Bacteria were cultured at 37°C for 24 h on Mueller Hinton Broth (Sigma-Aldrich) and fungi on Mueller Hinton Agar 2 (Sigma-Aldrich), and MICs were determined using Mueller Hinton Agar 2 (Sigma-Aldrich) and RPMI (Sigma-Aldrich). MIC testing was performed in 96-well sterile plates using a starting concentration of 256 µg/mL. The culture temperature was 37°C and the culture time was 24 hours.

2.7 Electric measurements

The representatives from the family of compounds was spin-coated (SPIN 150i, Polos) on unpatterned conductive substrate (ITO glass slide, Ossila Ltd). Investigated materials were compounds **1**, **2** and **4**. Also, one of the previously explored complexes was measured (**[Ag₃(3-cpy)₂(NO₂)₃]∞**.[17] The average thickness of films were 56 ± 8 nm. In the next preparation step the 100 nm thick Ag electrodes of the dimensions (1.3mm x 1.5mm) were sputtered (Leica EM

ACE600) at a top of the complex layer. In each case, the I-V curves characteristic measurements were conducted under an ambient atmosphere. Current–voltage characteristic (I–V) were performed on a Biologic SP-300 system with two electrodes connected to ITO substrate and Ag top electrodes, respectively. For the I–V measurements, the DC voltage sweep was executed - ranging the voltage limits alongside the scan velocities – see the following section.

2.8. Quantum chemical modelling

DFT calculations were performed using Gaussian 16 Revision C.01 software package using the B3LYP functional and TZVP basis set[27,28] in vacuum. Unconstrained optimisation of the molecular geometry was carried out under tight convergence criteria ($\Delta E_{SCF} \leq 10^{-8}$ hartree). Potential distribution maps were plotted using GaussView software package, version 5.0.8.

3. Results and discussion

3.1 Syntheses

As a result of the syntheses, we have obtained three coordination polymers **1**, **2**, **3** and one molecular complex **4** (Scheme I).
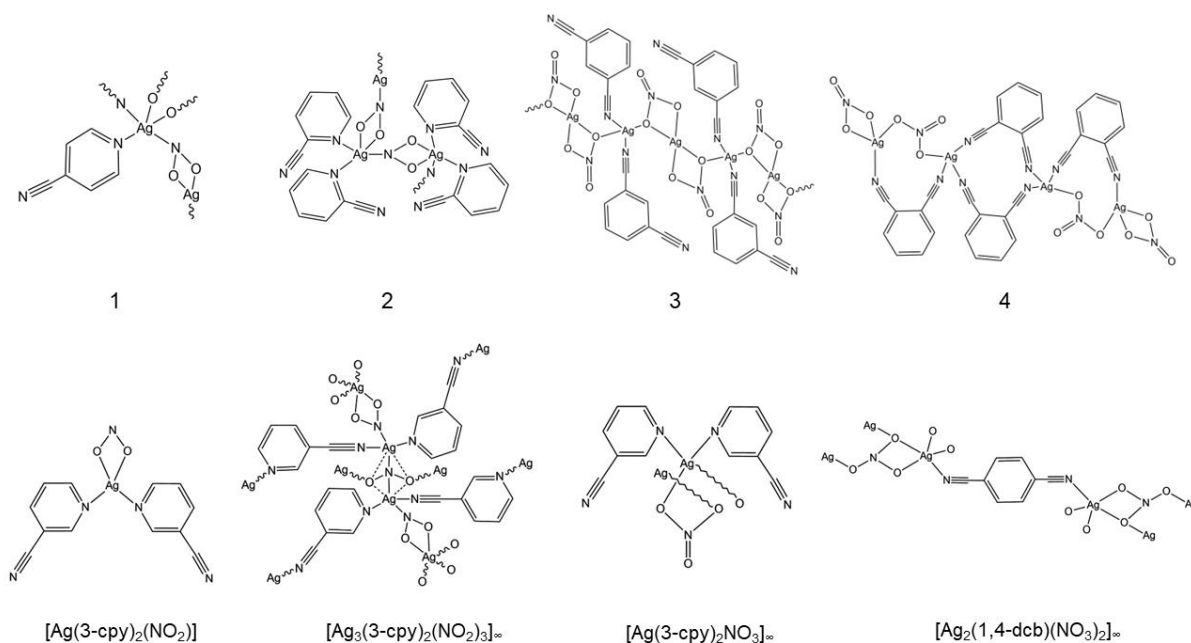
Scheme I. *Formulas of coordination polymers 1, 2, 3 and molecular complex 4 synthesized within this work (upper row); formulas of silver complexes with 3-cyanopyridine and 1,4-dicyanobenzene synthesized previously (lower row,*[17]*).*

The syntheses of the complexes were simple and required mixing of the reagents: $AgNO_2$ or $AgNO_3$ and nitrile in the appropriate solvents in the molar ratio 1 : 1. In the case of compound **3**, we did not find the conditions appropriate for the crystallization of the pure product. Using different solvents and molar ratios of the reactants we usually obtained 1,3-dcb ligand as the major product of

crystallization. Finally, the crystals of the complex **3** were separated under the optical microscope and suitable single-crystal for X-ray diffraction experiment was found allowing the crystal structure determination. In the Scheme I we also show the formulas of the complexes obtained previously [17], whose properties were studied within this paper.

3.2 Crystal structures

Compound **1** crystallizes in orthorhombic symmetry, space group $P2_12_12_1$ with one 2-cyanopyridine molecule and one nitrite ion in the asymmetric part of the unit cell (Figure 1a). The coordination number of silver is formally equal to 5 and the geometry is close to square pyramid as indicated by τ_5=0.01.[29] Three-dimensional pattern in the crystal structure of **1**, may be described as antiparallel chains connected either by nitrite ions (along *b* axis) or 4-cyanopyridine molecules (along *c* axis). The separation of silver atoms *via* nitrite is 5.218 Å and the distance between silver atoms linked by 4-cyanopyridine is 9.983 Å. The interchain Ag---Ag distances between the antiparallel chains are 6.659 Å. The packing and the chains within it are illustrated in Figure 1b.
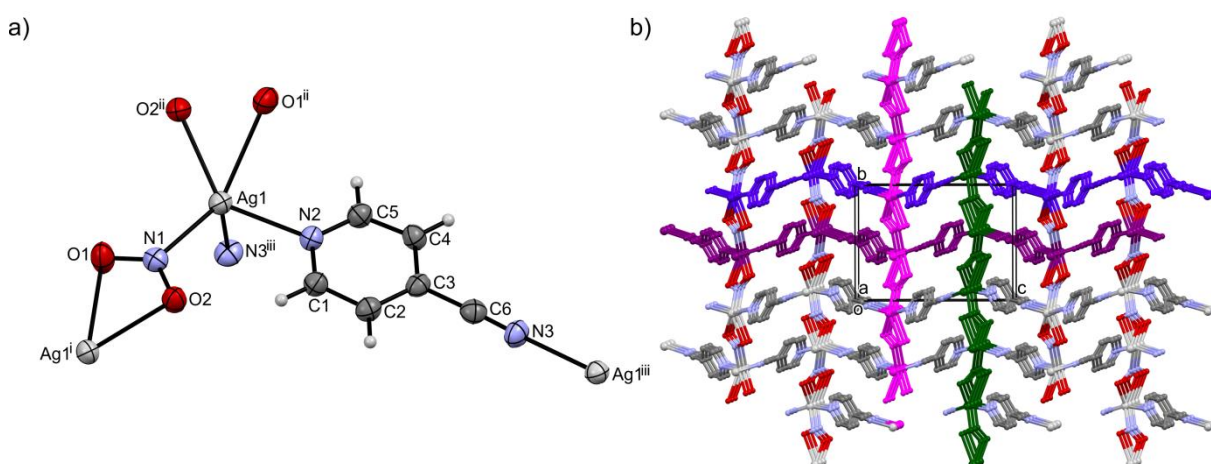

Figure 1. *Molecular structure of complex* **1**: *a) coordination sphere of the Ag(I) ion with the atomic numbering scheme, displacement ellipsoids drawn at 50% probability level. Important bond lengths [Å]: Ag1–N1 2.337(4), Ag1–N2 2.359(4), Ag1–O1^{ii} 2.595(4), Ag1–O2^{ii} 2.384(3), Ag1–N3^{iii} 2.362(4). Important angles [°]: N1–Ag1–N2 103.02(13), N1–Ag1–O1^{ii} 135.31(13), N1–Ag1–O2^{ii} 108.49(14), N1–Ag1–N3^{iii} 103.46(15), N2–Ag1–O1^{ii} 85.69(12), N2–Ag1–O2^{ii} 135.62(13), N2–Ag1–N3^{iii} 90.82(15), O1^{ii}–Ag1–O2^{ii} 49.94(11), O1^{ii}–Ag1–N3^{iii} 120.36(15), O2^{ii}–Ag1–N3^{iii} 110.8(1); symmetry operations: ^{i} =2-x, -1/2+y, 1.5-z, ^{ii} =2-x, 1/2+y, 1.5-z, ^{iii} =1/2-x, 1-y, ½+z; b) packing of polymeric structure, hydrogen atoms of pyridine ring removed for clarity; the antiparallel chains of silver atoms linked via nitrite ions indicated with magenta and green and these linked by 4-cyanopyridine drawn in purple and violet-blue.*

In complex **2** silver atom is coordinated by two molecules of 2-cyanopiridine and two bridging nitrite ions forming a distorted tetrahedral environment: τ_4 = 0.85, τ_4' = 0.82 (Figure 2a).[29,30] The nitrite ion bridges two silver ions *via* short bond Ag1–N5 2.262(7) Å, and long one Ag1–O1 2.66(1) Å. Silver atoms and nitrite ions form a skeleton of the 1-D coordination polymer which is propagated along the *c* crystallographic axis. The polymer exhibits a zig-zag configuration as shown in Figure 2b. The

shortest Ag1···Ag1 distance in the chain is 5.289(2) Å. The polymeric structure is stabilized by the π-π stacking interactions of the aromatic rings of the 2-cyanopyridine ligands of the neighboring chains (Figure 3).
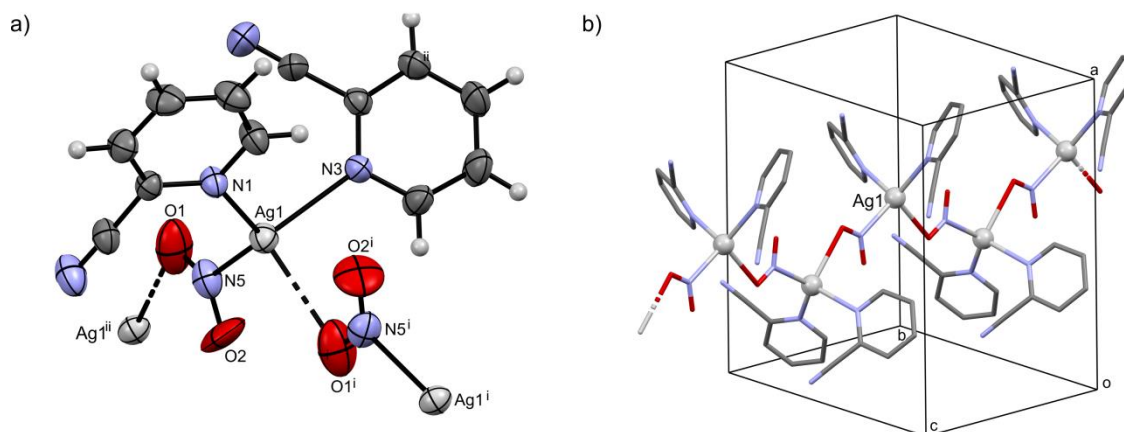

Figure 2. *Molecular structure of complex **2**: a) coordination sphere of the Ag(I) ion with the atomic numbering scheme, displacement ellipsoids drawn at 50% probability level. Important bond lengths [Å]: Ag1–N1 2.327(5), Ag1–N3 2.435(4), Ag1–N5 2.262(7), Ag1–O1^i 2.66(1). Important angles [∘]: N1–Ag1–N3 108.64(15), N1–Ag1–N5 125.1(2), N3–Ag1–N5 107.60(19), N1–Ag1–O1^i 115.01(30), N3–Ag1–O2^i 96.98(20), N5–Ag1–O2^i 99.69(30); symmetry operations: ^{i} =1-x, 1-y, -1/2+z, ^{ii} =1-x, 1-y, 1/2+z; b) 1-D polymeric structure, hydrogen atoms omitted for clarity.*
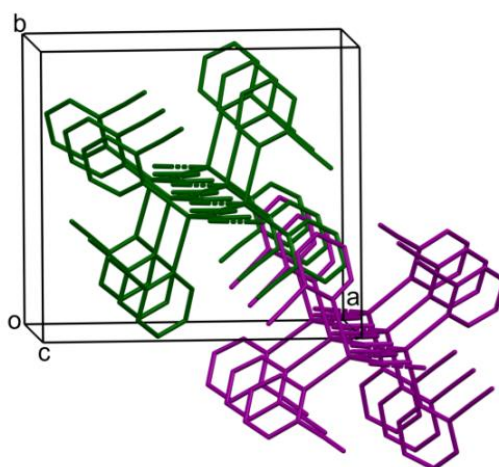

Figure 3. *Crystal packing of complex **2**; hydrogen atoms of pyridine ring removed for clarity, cell axes demonstrated; the parallel chains of silver atoms linked via nitrite ions indicated with magenta and green.*

Compound **3** has the one-dimensional polymeric structure of alternating cationic [Ag(1,3-dcb)$_2$]$^+$ units and [Ag(NO$_3$)$_2$]$^-$ anions. In the asymmetric part of the unit cell, two silver(I) ions of a distorted tetrahedral geometry are present (Figure 4a). The Ag1 atom is coordinated by two molecules of 1,3-dcb and two oxygen atoms from nitrate ions (τ_4 = 0.74, τ_4' = 0.63), whereas Ag2 atom is coordinated exclusively by the oxygen atoms of two nitrate ions (τ_4 =0.72 , τ_4' =0.69). Distorted coordination is affected by chelation of the nitrate anion in the asymmetric mode, where the longer Ag2–O5 bond is

2.560 Å long and the shorter one Ag2–O1 is equal to 2.300 Å. The Ag–O–N–Ag chain propagates along the *a* axis and exhibits a zigzag configuration characteristic for 1,4-dcb complexes of 11 group metals.[31] The shortest Ag⋯Ag separation within the chain is 4.840 Å and between the chains it is 3.708 Å, which, being longer than the sum of the van der Waals radii of silver atoms (3.44 Å[32]), excludes argentophilic interactions.[33] The arrangement of the polymer chains within the crystal is illustrated in Figure 4b.
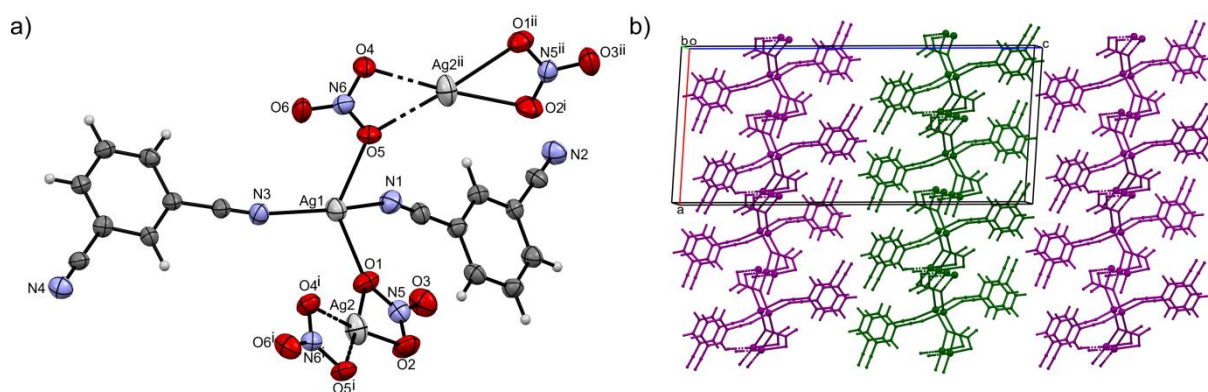

Figure 4. *Molecular structure of complex **3**: a) coordination spheres for two symmetry independent Ag(I) ions. Displacement ellipsoids drawn at 30% probability level. Important bond lenghts [Å]: Ag1–O1 2.558(15), Ag1–O5 2.519(14), Ag1–N1 2.198(16), Ag1–N3 2.208(15), Ag2–O1 2.574(17), Ag2–O2 2.398(18), Ag2–O4 2.418(12), Ag2–O5 2.567(14). Important angles: O1–Ag1–O5 109.1(4), O1–Ag1–N1 102.1(6), O1–Ag1–N3 99.9(5), O5–Ag1–N1 87.5(6), O5–Ag1–N3 108.8(5), N1–Ag1–N3 146.3(5), O1–Ag2–O2 51.0(5), O1–Ag2–O4 125.7(4), O1–Ag2–O5 176.3(5), O2–Ag2–O4 175.2(7), O2–Ag2–O5 132.6(5), O4–Ag2–O5 50.7(4); symmetry operations: i = 1/2+x, -2-y, z, ii = -1/2+x, -2-y, z; b) crystal packing viewed along b axis.*

Compound **4** crystallizes in the monoclinic crystal system, space group $P2_1/n$. It is a molecular, tetranuclear complex, in which four silver cations are bridged by four 1,2-dcb ligands (Figure 5a). The molecule lies on the inversion centre and therefore the asymmetric part of the unit cell contains two silver cations, two nitrate anions and two 1,2-dcb molecules. Both independent Ag1 and Ag2 ions feature C.N. = 4, with distorted geometries. Atom Ag1 is coordinated by one –C≡N group of 1,2-dcb and three oxygen atoms of two nitrates (one chelating). The geometrical indices of Ag1 are τ_4 = 0.61, τ_4' = 0.57. Atom Ag2 is coordinated by three –C≡N groups and one nitrate oxygen and its geometry is closer to tetrahedral (τ_4 = 0.77, τ_4' = 0.69). Ag–N bonds are in the range 2.178 Å to 2.333 Å, while Ag-O bonds fall within the range 2.431 – 2.496 Å. The important bond lengths and angles are given in Fig. 5 caption. "Wavy" molecules of **4** pack in piles parallel to axis *a* (Figure 5b). The intermolecular aggregation is stabilized by weak C–H⋯O hydrogen bonds between 1,2-dcb and nitrate – almost all C–H bonds of 1,2-dcb are engaged in relatively short H-bonds of this type (*e.g.* C5–H5⋯O1 $3.193_{C5⋯O1}/2.567_{H5⋯O1}$ Å). The interactions are reinforced by several Ag1⋯π contacts (*e.g.* Ag1⋯C6 3.225 Å) between the neighboring molecules. There are no close Ag⋯Ag contacts within or between the molecules.
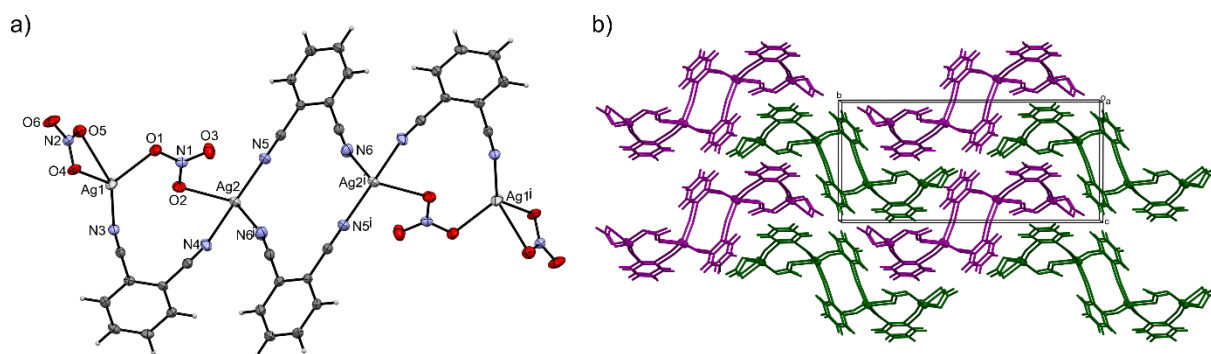
Figure 5 *Molecular structure of complex* **4**: *a) the molecule with the numbering scheme, displacement ellipsoids drawn at 50% probability level; important bond lenghts [Å]: Ag1–O1 2.4307(16), Ag1–O4 2.4262(15), Ag1–O5 2.4956(16), Ag1–N3 2.1783(19), Ag2–O2 2.4423(16), Ag2–N5 2.2116(19), Ag2–N6[i] 2.3330(19); Symmetry operations: [i] = 2-x, 1-y, 2-z; b) crystal packing viewed along a axis.*

3.3 FT-IR spectroscopy

IR spectroscopy was used to confirm the coordination behaviour of the nitrile ligands in the bulk samples. The FT-IR ATR spectra of complexes **1**–**4** compared to their respective ligands are presented in the Figs. 1S – 4S of Supplementary Information. In the absence of coordination to Ag$^+$ ions, we should expect a similar value of the stretching vibration of the nitrile group of the coordinated and free ligand; in the case of cyanopyridines, it means that they coordinate only via the N atom of the pyridine ring.[17,34] The direct coordination of the nitrile group to the metal ion, shifts the maximum of the band associated with the ν_{CN} mode in comparison to the uncoordinated nitriles.[17,35] Analysis of the FT-IR spectra of the ligands and their silver complexes **1**-**4** revealed that the differences in the nitrile stretching frequencies for cyanopyridines and their complexes are in accordance with the crystal structures. The characteristic frequencies are collected in Table 2.

Table 2 *The frequencies of the $\nu_{C\equiv N}$ stretching mode of free and complexed cyanopyridines and cyanobenzenes and complexes* **1**–**4**.

Compound	ν_{CN} [cm^{-1}]	$\Delta\nu_{C\equiv N}$ [cm^{-1}] vs. non-coordinated ligand	Comment
4-cpy	2235	–	
1	2250	+15	Coordinated nitrile
2-cpy	2243	–	
2	2236	-7	Non-coordinated nitrile
1,3-dcb	2234	–	
3	2264	+30	Coordinated nitrile
	2238	+4	Non-coordinated nitrile
1,2-dcb	2232	–	
4	2258	+26	Coordinated nitrile
	2245	+13	Coordinated nitrile

The FT-IR spectra of complexes **1** and **2** (cyanopyridine ligands) showed the presence of coordinated -C≡N group in complex **1** and a non-coordinated nitrile in the case of complex **2**. FT-IR spectrum of dicyanobenzene complex **3** features two distinct bands of nitrile stretching indicating the presence of

both coordinated (+30 cm^{-1}) and non-coordinated (+4 cm^{-1}) nitrile. In complex **4**, both nitrile groups are coordinated to silver ions and in the spectrum we observe two bands at +13 and +30 cm^{-1} compared to the FT-IR spectrum of the free ligand.

The bands due to v_a and v_s frequencies of nitrite are seen at about 1365-1332 and 1264-1235 cm^{-1} respectively and the bending frequency around 847-845 cm^{-1}.[36-38] The asymmetric (v_3, several bands centered at 1322 cm^{-1}) and symmetric (v_1, around 1040 cm^{-1}) modes of nitrates **3** and **4** split into several bands, especially in complex **4**, which features both bridging and terminal nitrate ions (Figures 5, 3S and 4S).

3.4 Thermal stabilities

Thermal stability was studied for **1-2**, **4** and silver complexes described previously: **[Ag(3-cpy)₂(NO₂)]**, **[Ag₃(3-cpy)₂(NO₂)₃]∞**, **[Ag(3-cpy)₂NO₃]∞**, **[Ag₂(1,4-dcb)(NO₃)₂]∞** [17] in air and N$_2$ atmosphere. The TGA and DTA data for all compounds are presented in Figs. 5S – 22S and summarized in Tables 1S and 2S of Supporting Information.

Analysing the stability of compounds derived from substrates such as AgNO$_3$ containing cyanopyridine and dicyanobenzene molecules, we should expect endothermic effects to accompany the decomposition of the complexes. Previous studies have shown that AgNO$_3$ itself can decompose via different pathways, which may lead to the formation of diverse products.[39,40] The main, confirmed, one-step decomposition pathway leads to metallic silver, nitrogen oxides NO$_2$, NO, metallic silver nanoparticles and molecular oxygen.[40] The other products: N$_2$ and N$_2$O, silver oxide/silver nitrate complex suggested by Paulik and coworkers[39] were not confirmed later by Otto.[40] The DTA curve of AgNO$_3$ shows two endothermic peaks at about 165 and 210°C. The latter peak was ascribed to the melting of the compound and the lower peak is likely connected with a polymorphic transition.[39-41] In the case of TG and DTG curves, complete decomposition of the liquified compound is observed between 360-500°C, with the final endothermic peak at 500°C and formation of Ag, irrespective of the atmosphere applied in the experiment.[40] The thermal analysis of AgNO$_2$ shows that decomposition process starts at 120°C/128°C and results initially in silver(I) oxide and nitrogen oxides NO and NO$_2$.[42,43] At this elevated temperature the released nitrogen oxides react quickly with the silver(I) oxide producing silver nitrate.[42]

On the other hand, for metal complexes with cyanopyridines TG and DTA curves were characterized by three endothermic peaks attributed to the partial release of cyanopyridine molecules from the compound structure.[44,45] In the case of complexes containing dicyanobenzene molecules, TG/DTA diagrams with three peaks were also obtained, however the loss of dcb molecule was associated with only one of the decomposition peaks between 118 and 175°C.[46,47]

The complete TG, DTG and DTA data for the studied complexes are placed in Supplementary materials. The TG and DTG curves revealed a very complex way of thermal decomposition of the

studied complexes. The obtained DTA data showed that some or even all of the decomposition processes are exothermic reactions, which differs significantly from the literature data. These exothermic steps were observed both for the air and in the protective atmosphere of nitrogen thus the oxidation by the oxygen was excluded.[48,49] However, it is very probable that the exothermic effects are due to the reactions between the released oxidizing nitrogen oxides and the organic nitriles. Additionally the silver ions may have a catalytic effect on the reactions as the transiently formed silver(I) oxide is a long-recognized oxidation agent.[50,51]

Compound **1** decomposes in three steps (Figs. 5S and 6S). Decomposition begins above 110 °C with the release of nitrogen oxides and partial release of 4-cpy. It is represented by a sharp, exothermic gradient in the DTA curve with a maximum at 153 °C. The second stage of decomposition occurs at 226-327°C and is accompanied by the loss of 4-cpy. The third stage, which led to the final decomposition of complex **1**, occurred at temperatures above 327°C. The slight mass loss is probably associated with the release of oxygen from the resulting Ag_2O molecule. It is evident from the DTA curve that the two final stages were exothermic – either almost unnoticeably (T_{max} not defined) or strongly ($T_{max\ DTA}$=344°C).

A similar decomposition pattern was observed for complex **2** and silver nitrite coordination polymer **$[Ag_3(3\text{-cpy})_2(NO_2)_3]_\infty$**, where the first stage on the DTG curve was characterized by a sharp gradient and two smaller peaks for the other stages (Figs. 7S-10S). The decomposition of complex **2**, starts above 71°C with a maximum of DTA 122°C, the second process undergoes at 152-290°C ($T_{max\ DTA}$=260°C) and third stage begins at 299°C ($T_{max\ DTA}$=391°C). The weight loss of the first stage corresponds to the evolution of nitrogen oxides, mainly NO, and the release of one molecule of 2-cpy. In further stages, a partial release of 2-cpy is observed. The decomposition of **$[Ag_3(3\text{-cpy})_2(NO_2)_3]_\infty$**, begins above 80°C ($T_{max\ DTA}$=155°C) with the detachment of the nitrite group and the 3-cpy fragment (Figs. 9S and 10S). The subsequent steps are characterized by a small mass loss associated with further decomposition of the organic ligand. The second step corresponds to the temperature range 190-287 ($T_{max\ DTA}$=286°C), and third undergoes within 293-350 °C ($T_{max\ DTA}$=320°C).

Finally, regarding the thermal stability of silver nitrite complexes, we have analyzed the thermal decomposition process of molecular silver nitrite, cyanopyridine complex **$[Ag(3\text{-cpy})_2(NO_2)]$**. Contrary to coordination polymers described above, molecular **$[Ag(3\text{-cpy})_2(NO_2)]$** featured two endothermic processes at lower temperatures, which may correspond to phase transitions such as melting and evaporation (Figs. 11S and 12S). At higher temperatures again the exothermic reactions are observed with $T_{max\ DTA}$ at 152°C and 336°C. In comparison to coordination polymers of the similar composition it is apparent that the molecular compound is less thermally stable, *i.e.* the changes begin in the lower temperature. Additionally, when we repeated the measurement in the protective atmosphere

of nitrogen the degradation was less complex and the exothermic effects were less pronounced thus we conclude that in the elevated temperature the complex reacts with oxygen (Figs. 13S and 14S).

The decomposition of nitrate complex **4** in the atmosphere of air, illustrated in Figs. 15S and 16S, begins at 131°C and this first stage ends at 249°C ($T_{max\,DTA}$=247°C); further weight loss occurs between 250-310°C ($T_{max\,DTA}$=306°C). On the DTA diagram at least one endothermic and two exothermic peaks are clearly visible. The endothermic peak at 134°C (DTA) roughly corresponds to the melting point determined by the usual method (128.5-129°C). Each step of the loss of weight is accompanied by the exothermic peak on the DTA at 247 and 306°C. Interestingly the results of the TG/DTG analysis of **4** in N_2 atmosphere were very similar (Figs. 17S and 18S), which confirms that the exothermic reactions undergo within the decomposing complex without the participation of oxygen.

For comparison we performed and describe the TG and TA analysis of two more nitrate silver coordination polymers with nitrile ligands: **[Ag(3-cpy)$_2$NO$_3$]$_\infty$** and **[Ag$_2$(1,4-dcb)(NO$_3$)$_2$]$_\infty$**.[17] Both compounds decomposed in a similar manner but differently from molecular **4**. The three distinct steps of weight loss were accompanied by a two endothermic and one exothermic peaks in the DTA chart (Figs. 19S-22S).

At the end of this chapter, we would like to indicate one more feature that differentiates the behavior of the described silver complexes during thermal analysis. In the most cases the mass percentage of the residue after thermal decomposition roughly corresponds to the metallic silver as in nitrites: **2**, **[Ag$_3$(3-cpy)$_2$(NO$_2$)$_3$]$_\infty$**, **[Ag(3-cpy)$_2$(NO$_2$)]** or silver oxide as in nitrates: **[Ag(3-cpy)$_2$NO$_3$]$_\infty$** and **[Ag$_2$(1,4-dcb)(NO$_3$)$_2$]$_\infty$**. There are two compounds that definitely do not follow this pattern: complex **1** in which the residue is 30% instead of 42% anticipated for metallic silver and compound **4**, which is volatile since the solid residue is merely 6,4% instead of calculated 26% (Table 1S).

3.5 Antibacterial and antifungal activity

Antimicrobial tests were performed for complexes **1**, **2**, **4** as well as **[Ag(3-cpy)$_2$(NO$_2$)]**, **[Ag$_3$(3-cpy)$_2$(NO$_2$)$_3$]$_\infty$**, **[Ag(3-cpy)$_2$NO$_3$]$_\infty$**, **[Ag$_2$(1,4-dcb)(NO$_3$)$_2$]$_\infty$**.[17] All compounds demonstrated relatively good antifungal and antibacterial activity with the MICs values in the 1-64 µg/mL range (Table 3). Coordination polymer **[Ag$_3$(3-cpy)$_2$(NO$_2$)$_3$]$_\infty$** exhibited the highest activity - it effectively inhibited the growth of *P. aeruginosa* at the concentration of 8 µg/mL which is 3-fold lower than MIC value of AgNO$_2$. Satisfactory antibacterial properties were also displayed by complex **1** and molecular complex **[Ag(3-cpy)$_2$(NO$_2$)]**. Both these complexes inhibited growth of *P. aeruginosa* at the concentration 16 µg/mL which is 2 times lower than AgNO$_2$. Complexes **2**, **4** and **[Ag(3-cpy)$_2$NO$_3$]$_\infty$** exhibited the same or even lower activity than AgNO$_2$ and AgNO$_3$. Other strains of bacteria exhibited slightly higher resistance to the activity of the studied complexes. With the exception of *S. enteritica* and complex **[Ag$_3$(3-cpy)$_2$(NO$_2$)$_3$]$_\infty$** (MIC=128 µg/mL), the MIC values of all compounds were in the range from 16 to 64 µg/mL, comparable to MIC values of AgNO$_2$ and AgNO$_3$.

Table 3 *Results of Antibacterial activity of Ag(I) complex – MIC.*

Ag(I)complex	Gram (+) S. aureus ATCC 25923	Gram (+) S. aureus ATCC 29213	Gram (-) P. aeruginosa ATCC 27853	Gram (-) E. coli ATCC 25922	Gram (-) S. enterica PCM 2266	Fungi C. albicans SC 5314	Fungi C. glabrata DSM II 226
1	32	16	16	32	32	2	2
2	32	16	32	32	32	2	2
4	32	32	32	32	64	16	32
$[Ag(3\text{-}cpy)_2(NO_2)]$	64	64	16	64	128	2	4
$[Ag_3(3\text{-}cpy)_2(NO_2)_3]_\infty$	32	32	8	32	64	1	2
$[Ag(3\text{-}cpy)_2NO_3]_\infty$	64	64	64	64	32	2	4
$[\{Ag(1,2\text{-}dcb)_4\}(NO_3)_4]$	32	32	32	16	32	2	2
$AgNO_2$	32	16	32	32	16	2	2
$AgNO_3$	16	32	32	8	16	1	1
3-cpy/2-cpy/ 4-cpy/ 1,2-dcb/1,4-dcb	>256	>256	>256	>256	>256	>256	>256

The Minimum inhibitriy concentration (MIC) [µg/mL] header spans all pathogen columns.

Table 4 *Results of Antibacterial activity of Ag (I) complex - inhibition zone diameter (mm).*

Ag(I)complex	Bacteria Gram (+) S. aureus ATCC 25923	Bacteria Gram (+) S. aureus ATCC 29213	Bacteria Gram (-) P. aeruginosa ATCC 27853	Bacteria Gram (-) E. coli ATCC 25922	Bacteria Gram (-) S. enterica PCM 2266	Fungi C. albicans SC 5314	Fungi C. glabrata DSM II 226
1	13	8	14	8	20	20	24
2	8	7	13	7.1	20	16	18
4	12	10	14	9.5	24	15	18
$[Ag(3\text{-}cpy)_2(NO_2)]$	7.5	7.5	14	9.5	24	24	18
$[Ag_3(3\text{-}cpy)_2(NO_2)_3]_\infty$	14	8	15.5	10	24	20	17
$[Ag(3\text{-}cpy)_2NO_3]_\infty$	7	7	11	10	24	21	17
$[Ag_2(1,4\text{-}dcb)(NO_3)_2]_\infty$	8	7	14	9	23	14	17
$AgNO_2$	8	7	13	10	22	14	14
$AgNO_3$	10	7	13.5	10	23	16	16
3-cpy/2-cpy/ 4-cpy/ 1,2-dcb/1,4-dcb	0	0	0	0	0	0	0

Considering the MIC values, the highest activity was observed against two fungal pathogens *C. albicans* and *C. glabrata*. Almost all compounds effectively inhibited growth of fungal strains at concentrations of 1-4 µg/mL. Only molecular complex **$[Ag(3\text{-}cpy)_2(NO_2)]$** was less active (MIC 16 or 32 µg/mL). However, it should be emphasized that *C. albicans* and C. *glabrata* exhibited higher susceptibility to $AgNO_2$ and $AgNO_3$ (MICs in the range 1-2 µg/mL).

Interestingly, in a different type of assay, *i.e.* disc-diffusion, the studied complexes revealed selective, high activity against *S. enteritica* with diameter zones in the range 20-24 mm, which is importantly larger value compared to other investigated strains of bacteria (Table 4). Another interesting result of this part of the study is the increased antifungal activity of nitrile complexes compared to $AgNO_2$ and $AgNO_3$. The remaining results of the agar disc-diffusion method are in agreement with the dilution MIC assay *e.g.* high activity against *P. aeruginosa*, particularly in the case of complex **[Ag_3(3-cpy)_2(NO_2)_3]_∞** (Tables 3 and 4).

3.6. Electrical characterization of thin films

Regarding potential application of synthesized compounds, outside antibacterial functionality scope, all of measured nitrile silver complexes showed non-linear electrical behaviour in a form of narrow, pinched I-V hysteresis loops. Typically in literature these are called hysteresis curves, and are associated to memristive, resistive switching behaviour. As can be concluded from Figure 6, in order register a non-linear response, particular potential threshold must be exceeded. In case of **1** for smaller window (Figure 6a) only linear response exists, whereas the non-linear hysteretic response can be measured for the potential window spanning from <-6 V; +6V> (Figure 6b). In other words – sample behaves as a typical resistor within narrower potential window, whereas extension of this window brings about hysteretic behaviour. This indicated the redox-type behaviours of the metal/complex interface. Despite minimal fluctuation of the switching points, in each individual measurement two distinguishable states of the devices can be found – either it is low resistivity state (LRS, higher current for defined voltage) or high resistivity state (HRS).
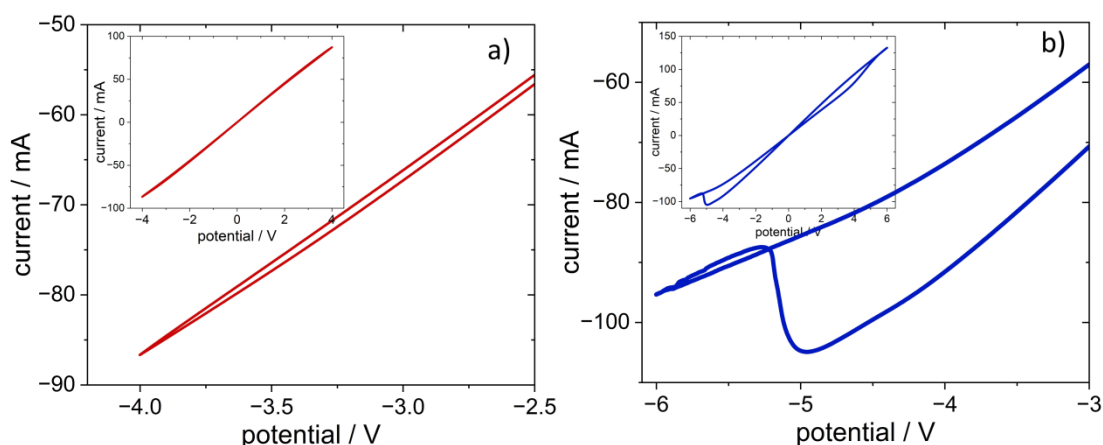

Figure 6. *Electric characterization of the thin film samples of compound **1**: a) range +/-4V and b) range +/- 6V. Each Figure depicts results taken with 100 mV/s velocity scans after several cycles of pre-conditioning with lower voltages than showed. Insets demonstrate results of the full range scans.*

From the electrical point of view, the most interesting compound to measure, happens to be complex **1**. Hysteresis is clearly visible (Figure 6b) with additional either capacitance or fractional memristance signals occurring upon measurement in quadrant III.[52,53] These results indicate that at least resistive switching processes[54] is responsible for resistive switching. It cannot be the formation of metallic filament (electrode material), though. In such a case the ratio (on/off ratio) between resistivity in HRS and resistivity in LRS would reach 10^4 or even more This effect disqualifies studied materials for memory application, where high ON/OFF ration is required. Fortunately, even low on/off efficient cases of thin film-materials serving information processing purposes.[55]

These rather narrow hysteresis loops can be better visualized and analysed upon subtraction of linear (Ohmic component), which was approximated by a homogeneous linear function. The residuals of this fittings are presented in Figure 7. Thus the obtained hysteresis curves indicate memristive character of all devices: a pinched hysteresis loop, with significantly asymmetric lobes. This asymmetry, along with the differences of maximum and minimum currents (cf. Fig. 6) suggests a leaky Schottky-barrier character of obtained junctions. The asymmetry factors (current ratio for
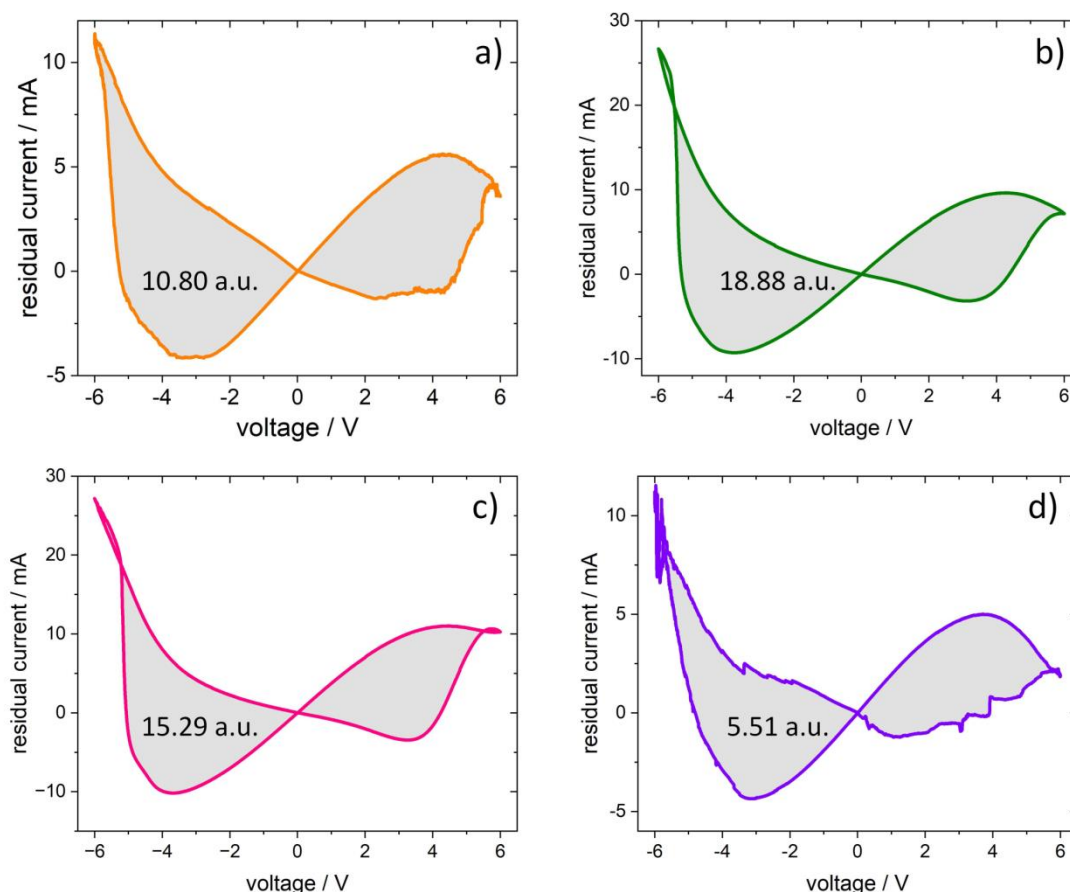

Figure 7. *Conductivity hysteresis presented as a residual current for silver complexes with cyanopyridines and 1,2-dcb: a) complex **2** (with 2-cpy); b) [Ag₃(3-cpy)₂(NO₂)₃]∞; c) complex **1** (with 4-cpy); and d) complex **4** (with 1,2-dcb). Numbers indicate the total surface area of hysteresis loop.*

forward and reversed bias voltages) are low (1.13, 1,36 and 1,42 for 2-, 3-, and 4-cyanopyridine complexes, respectively) but indicate weak current rectification. For 1,2-dicyanobenzene complex **4** this effect is even smaller (1.11). The memristive character of these junction can be quantified by the total surface area within the hysteresis loop. The highest value (18.86 a.u.) was recorded for 3-cyanopyridine complex **[Ag₃(3-cpy)₂(NO₂)₃]∞**, whereas 1,2-dicyanobenzene complex **4** presented the lowest value (5.51 a.u.). Interestingly, hysteresis curves recorded for 3-cyanopyridine and 4-cyanopyridine complexes show multiple cross points, which indicates contribution of capacitive effects or ferroelectric ordering during voltage scans. Taking into account that one crossing point is always present at U = 0 V, the second possibility seems to be more justified.[56,57] Furthermore, some theoretical studies relate these multiple cross points to memductance.[58]

Similarity in slope values of these fits, along with almost the same thickness of the layer (56 ± 8 nm) indicate very similar specific conductivity of studied compounds. It is justified by similar composition. Log-log plots (Figure 8) indicate mostly Ohmic character of electron transport in these materials (current-voltage slope in log scale equals to unity), however at voltages higher than 4V significant contribution from trap-assisted space-charge limited conductivity (SCLC) can be postulated on the basis of significantly higher slopes (1.17, 1.24 and 1.41 for 2-, 3-, and 4-cyanopyridine complexes, respectively). In the case of 1,2-dicyanobenzene the unity slope was observed in the whole voltage range. Slopes significantly higher that unity indicate quadratic dependence of current versus voltage, characteristic for space-charge limited current transport mechanism, therefore they are layer called SCLC exponents.
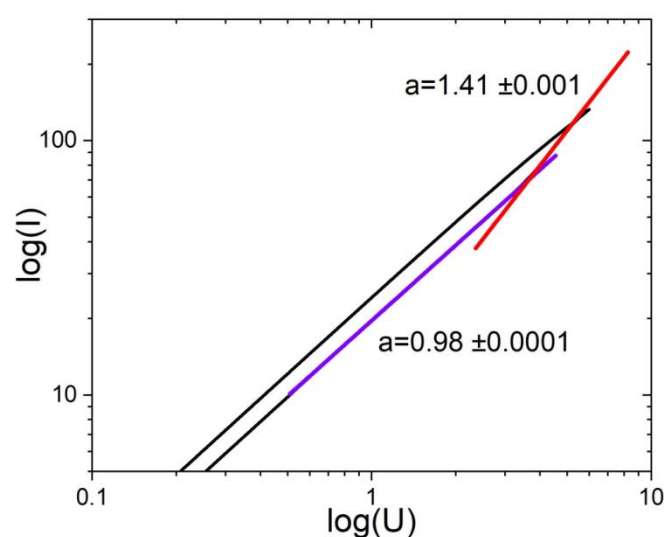

Figure 8. *Log-log plot of current-voltage characteristics for 4-cyanopyridine complex **2**.*

The similarities in electrical properties of all cyanopyridine derivatives originate from similarities of ligand structures and properties, as well as some analogies in binding motifs. The most significant

difference in all studied ligands are their charge distributions and resulting dipole moments (Figure 9). In all cases nitrile groups bear a significant negative change, the same is also observed for heteroatoms. Various arrangements of substituents in respect to heteroatoms result in a substantial changes in dipole moment and inhomogeneity of electric potential within the crystals. These inhomogeneities, in turn, influence charge transport and charge trapping phenomena at metal/layer interface.[59]
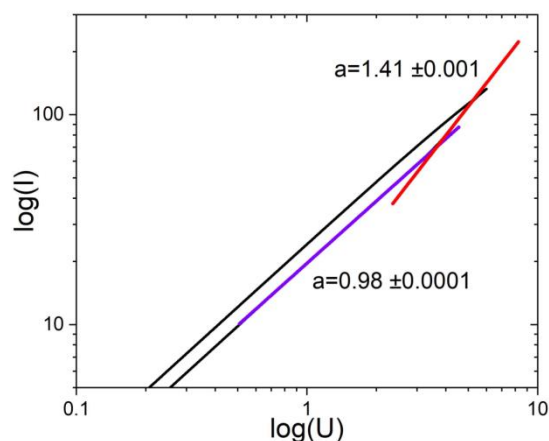

Figure 9. *Electrostatic potential distribution maps projected over total electron density for: a) 2-cyanopyridine; b), 3-cyanopyridine; c), 4-cyanopyridine; d) and 1,2-dicyanobenzene. Numbers indicate dipole moment of these molecules as calculated at the B3LYP/TZVP level.*
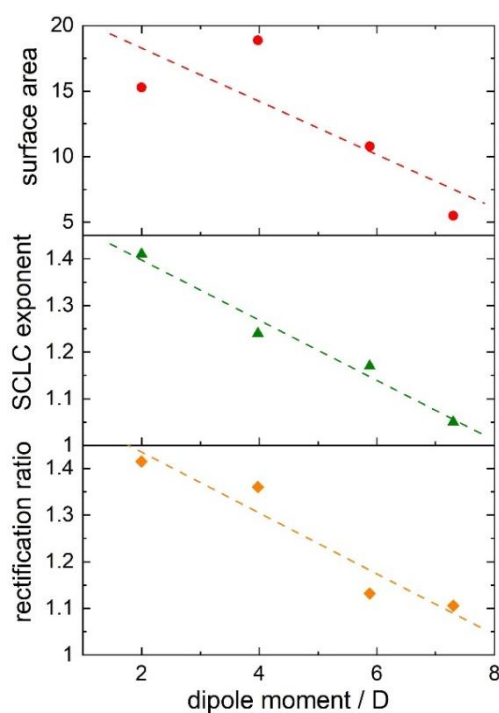

Figure 10. *Correlation of some electrical properties of Ag/complex/ITO junctions with dipole moments of ligands.*

It can be noted, that all physical quantities related to electrical properties of silver complex layers correlate with dipole moments of ligands: surface area of hysteresis loops decreases with increasing dipole moment, the same concerns the SCLC exponent (cf. Figure 8) and the rectification properties of Schottky junctions (Figure 10).

At current stage of research it is difficult to unambiguously assign this dependence to one particular process, but putatively, correlation with dipole moments indicates the role of electric fields variations at molecular level, along the conductivity path, as well as the height of the Schottky barrier at the silver/material interface.

4. Summary and conclusions

In this work we have described four new silver complexes nitrite/nitrate with two types of nitrile ligands: cyanopyridines and cyanobenzenes. We have studied the thermal properties of these new and other similar silver complexes to conclude that these compounds are not thermally stable and show complicated pattern of decomposition involving probably oxidation reactions between nitrite/nitrate ions and nitrile ligands. On the other hand, the studied nitrile complexes of silver show excellent antimicrobial and antifungal properties as anticipated by the weak binding and facile release of silver ions from the nitrile complex.

Along with antimicrobial activity, interesting electrical phenomena have been observed and related with the electronic structure of organic ligands. All these makes the silver/nitrile systems a fascinating sandbox, in which self-assembly of low-stability complexes yields materials with diverse prospective applications in biological studies and molecular/organic electronics.

6. Conflicts of Interest

The authors declare that they have no known competing financial interests or personal relationships that could have appeared to influence the work reported in this paper.

7.References

[1] S. Medici, M. Peana, V. M. Nurchi, M. A. Zoroddu, *J. Med. Chem.* **2019**, 62, 5923.

[2] H. Nishida, H. M. Risemberg, *Pediatrics*, **1975**, 56, 368.

[3] R. Rowan, T. Tallon, A. M. Sheahan, R. Curran, M. McCann, K. Kavanagh, M. Devereux, V. McKee, *Polyhedron* **2006**, 25, 1771.

[4] J. Kuchar, J. Rust, C. W. Lehmann, F. Mohr, *Inorg. Chem.* **2020**, 59, 10557.

[5] D. Leaper, *Int. Wound J.* **2012**, 9, 461.

[6] S. Medici, M. Peana, G. Crisponi, V. M. Nurchi, J. I. Lachowicz, M. Remelli, M. A. Zoroddu, *Coord. Chem. Rev.* **2016**, 327–328, 349.

[7] S. Y. Liau, D. C. Read, W. J. Pugh, J. R. Furr, A. D. Russell, *Lett. Appl. Microbiol.* **1997**, 25, 279.

[8] P. O. Asekunowo, R. A. Haque, M. R. Razali, S. W. Avicor, M. F. F. Wajidi, *Eur. J. Med. Chem.* **2018**, 150, 601.

[9] M. O. Karataş, N. Özdemir, M. Sarıman, S. Günal, E. Ulukaya, İ. Özdemir, *Dalton Trans.* **2021**, 50, 11596.

[10] A. Pavic, N. D. Savić, B. Đ. Glišić, A. Crochet, S. Vojnovic, A. Kurutos, D. M. Stanković, K. M. Fromm, J. Nikodinovic-Runic, M. I. Djuran, *J. Inorg. Biochem.* **2019**, 195, 149.

[11] K. Nomiya, R. Noguchi, M. Oda, *Inorg. Chim. Acta* **2000**, 298, 24.

[12] J. Arduengo, H. V. R. Dias, J. C. Calabrese, F. Davidson, *Organometallics* **1993**, 12, 3405.

[13] W. Streciwilk, J. Cassidy, F. Hackenberg, H. Müller-Bunz, F. Paradisi, M. Tacke, *J. Organomet. Chem.* **2014**, 749, 88.

[14] D. A. Medvetz, K. M. Hindi, M. J. Panzner, A. J. Ditto, Y. H. Yun, W. J. Youngs, *Met. Based Drugs* **2008**, 2008, 384010.

[15] S. B. Aher, P. N. Muskawar, K. Thenmozhi, P. R. Bhagat, *Eur. J. Med. Chem.* **2014**, 81, 408.

[16] J. Han, N. Ye, X. Zhang, Z. Yu, J. Wang, Y. Zhang, Y. Wan, *Inorg. Chim. Acta* **2020**, 512, 119873.

[17] K. Gutmańska, A. Ciborska, Z. Hnatejko, A. Dołęga, *Polyhedron* **2022**, 220, 115831.

[18] T. Mazur, P. Zawal, K. Szaciłowski, *Nanoscale* **2019**, 11, 1080.

[19] J. Supniewski, *Preparatyka Nieorganiczna*, Polskie Wydawnictwo Naukowe, PWN, Warszawa, **1958**.

[20] STOE & Cie GmbH, X-Area 1.75, software package for collecting single-crystal data on STOE area-detector diffractometers, for image processing, scaling reflection intensities and for outlier rejection; **2015**, Darmstadt.

[21] G. M. Sheldrick, *Acta Crystallogr. Sect. C: Struct. Chem.* **2015**, 71, 3.

[22] O. V. Dolomanov, L. J. Bourhis, R. J. Gildea, J. A. K. Howard, H. Puschmann, *J. Appl. Crystallogr.* **2009**, 42, 339.

[23] L. J. Farrugia, *J. Appl. Crystallogr.* **2012**, 45, 849.

[24] C. F. Macrae, P. R. Edgington, P. McCabe, E. Pidcock, G.P. Shields, R. Taylor, M. Towler, J. van de Streek, *J. Appl. Crystallogr.* **2006**, 39, 453.

[25] CLSI. Performance Standards for Antimicrobial Susceptibility Testing; Seventeenth Informational Supplement; CLSI document M100–S17; Clinical Laboratory Standard Institute: Wayne, PA, USA, **2007**.

[26] J. H. Rex, Reference Method for Broth Dilution Antifungal Susceptibility Testing of Yeasts; Approved Standard—Third Edition; CLSI Document M27-A3; Clinical & Laboratory Standards Institute: Wayne, PA, USA, **2008**.

[27] A. Schaefer, H. Horn, R. Ahlrichs, *J. Chem. Phys.* **1992**, 97, 2571.

[28] A. Schaefer, C. Huber, R. Ahlrichs, *J. Chem. Phys.* **1994**, 100, 5829.

[29] A. W. Addison, T. N. Rao, J. Reedijk, J. van Rijn, G. C. Verschoor, *J. Chem. Soc., Dalton Trans.* **1984**, 7, 1349.

[30] A. Okuniewski, D. Rosiak, J. Chojnacki, B. Becker, *Polyhedron* **2015**, 90, 47.

[31] M. K. Broderick, C. Yang, R. D. Pike, A. Nicholas, D. May, H. H. Patterson, *Polyhedron* **2016**, 114, 333.

[32] A. Bondi, *J. Phys. Chem.* **1964**, 68, 441.

[33] H. Schmidbaur, A. Schier, *Angew. Chem. Int. Ed.* **2015**, 54, 746.

[34] H. Zhao, A. Bodach, M. Heine, Y. Krysiak, J. Glinnemann, E. Alig, L. Fink, M. U. Schmidt, *CrystEngComm* **2017**, 19, 2216.

[35] S. Wöhlert, I. Jess, U. Englert, C. Näther, *CrystEngComm* **2013**, 15, 5326.

[36] K. J. Rao, C. N. R. Rao, *J. Mater. Sci.* **1966**, 1, 238.

[37] K. C. Patil, R. K. Gosavi, C. N. R. Rao, *Inorg. Chim. Acta* **1967**, 1, 155.

[38] K. H. Stern, *J. Phys. Chem. Ref. Data* **1972**, 1, 747.

[39] F. Paulik, J. Paulik, M. Arnold, *Thermochim. Acta* **1985**, 92, 787.

[40] K. Otto, I. Oja Acik, M. Krunks, K. Tõnsuaadu, A. Mere, *J. Therm. Anal. Calorim.* **2014**, 118, 1065.

[41] W. L. Fraser, S. W. Kennedy and G. F. Taylor, *Acta Crystallogr. B* **1977**, B33, 311.

[42] T. M. Oza, V. T. Oza, R. H. Thaker, *J. Chem. Soc.* **1955**, 2457.

[43] K. C. Patil, C. N. R. Rao, *Inorg. Nucl. Chem. Lett.* **1966**, 2, 329.

[44] M. Heine, L. Fink, M. U. Schmidt, *CrystEngComm* **2018**, 20, 7556.

[45] M. Heine, L. Fink, M. U. Schmidt, *CrystEngComm* **2020**, 22, 2067.

[46] T. Niu, J. Lu, G. Crisci, A. J. Jacobson, *Polyhedron*, **1998**, 17, 4079.

[47] J. Han, Q. Gao, Z. Yu, X. He, C. Y. Quan, M. Munakata, *Inorg. Chim. Acta* **2014**, 423A, 340.

[48] R. Gunawan, S. Freij, D. K. Zhang, F. Beach, M. Littlefair, *Chem. Eng. Sci.* **2006**, 61, 5781.

[49] A. Kumar, E. E. Wolf, A. S. Mukasyan, *AIChE J.* **2011**, 57, 2207.

[50] A. Nagy, G. Mestl, *Appl. Catal. A* **1999**, 188, 337.

[51] H. Ehrich, W. Schwieger, K. Jähnisch, *Appl. Catal. A* **2004**, 272, 311.

[52] G. Zhou, J. Wu, L. Wang, B. Sun, Z. Ren, C. Xu, Y. Yao, L. Liao, G. Wang, S. Zheng, P. Mazumder, S. Duan, Q. Song, *Nanoscale* **2019**, 11, 17222-17229.

[53] E. M. Hamed, M. E. Fouda, A. G. Radwan, Conditions and Emulation of Double Pinch-off Points in Fractional-order Memristor. *2018 IEEE International Symposium on Circuits and Systems (ISCAS)*, Florence, Italy, **2018**, 1-5.

[54] Z. Wang, H. Wu, G.W. Burr, C. S. Hwang, K. L. Wang, Q. Xia, J. J. Yang, *Nat. Rev. Mater.* **2020**, 5, 173.

[55] E. Wlaźlak, D. Przyczyna, R. Gutierrez, G. Cuniberti, K. Szaciłowski, *Jpn. J. Appl Phys.* **2020**, 59, SI0801.

[56] D. Biolek, V. Biolkova, Z. Kolka, Memristor pinched hysteresis loops: Touching points, Part I. *2014 International Conference on Applied Electronics*, Pilsen, Czech Republic, **2014**, 37-40.

[57] K. Bhardwaj, M. Srivastava, *Analog Integr. Circ. Sig. Process.* **2022**, 110, 63.

[58] K. Bhardwaj, M. Srivastava, *Circuit World* **2022**, 48, 160.

[59] S. Braun, W. R. Salaneck, M. Fahlman, *Adv. Mater.* **2009**, 21, 1450.